

Radiative Characteristics at 89 and 36 GHz for Satellite-Based Cloud Water Estimation Over Land

Rie Seto¹, Kentaro Aida, Toshio Koike, and Shinjiro Kanae

Abstract—Satellite-based passive microwave (PMW) remote sensing is an essential technique to clarify long-term and large-scale distribution patterns of cloud water content (CWC). However, most CWC estimation methods are not implemented over land because of high heterogeneity of land radiation, and the detailed characteristics of microwave (MW) radiative transfer between land and atmosphere including clouds have not been elucidated. This study aims to elucidate these characteristics and reveal the accuracy of land emissivity representation necessary for adequate CWC estimation over land using satellite-based PMW under various CWC conditions. First, important parameters related to MW radiative transfer between land and atmosphere at CWC-relevant frequencies in the presence of clouds are determined theoretically. Next, the relationship between errors in these parameters and the brightness temperatures used for CWC estimation is clarified through considerations based on radiative transfer equations. Then, ground-based PMW observations and numerical simulation are used to reveal the actual values of these important parameters and the size of errors. Finally, the results show that for any cloud liquid water path (LWP) value greater than 1.6 kg/m^2 at 89 GHz and 5 kg/m^2 at 36 GHz, we can reasonably neglect the heterogeneity of emissivity and radiation from the land surface for CWC estimation. However, when LWP values are below the threshold, the error in the representation of land emissivity should be kept below 0.015 for both 89- and 36-GHz data, and volumetric soil moisture content should have an error lower than 5%–6% for both frequencies.

Index Terms—Cloud water content (CWC) retrieval over land, passive microwave (PMW) remote sensing, representation of land emissivity.

I. INTRODUCTION

SATELLITE-BASED passive microwave (MW) remote sensing (PMW) provides valuable opportunities for global estimation of cloud water content (CWC) in extensive cloud systems and investigation of its role in large-scale energy and

water cycling. For example, O'Dell *et al.* [1] constructed an 18-year data set of cloud liquid water path (LWP) values determined using satellite-based PMW sensors and used it to investigate climatology. The climatology results showed stronger diurnal cycles of LWP values than those of cloud fractions in coastal regions and stratocumulus regions. Elsaesser *et al.* [2] developed a 29-year data set of LWP values and total water path values, updating climatology through the aggregation of 14 PMW retrieval products. These climatologies are expected to provide novel understandings of various climatic factors that are important in cloud-climate feedback, such as rainfall in the intertropical convergence zone, South Pacific convergence zone, and El Niño-Southern Oscillation. These data sets and retrieval techniques can also be used to evaluate or constrain climate models. Lauer *et al.* [3] validated LWP representation in Earth-system models using satellite-based PMW LWP data and revealed that the updated versions of the Earth system models showed reduced intermodel spread for cloud LWP data.

Many currently available methods of CWC estimation using satellite-based PMW measurements estimate by inversely solving radiative transfer models (RTMs) (e.g., Liu and Curry 1993 [4], Greenwald *et al.* [5], Lin and Rossow [6], Weng and Grody [7], Kummerow *et al.* [8], and Hilburn and Wentz [9]), which physically represent the radiative transfer processes in the atmosphere and simulate satellite-observed radiative measurements. Retrieval algorithms often implement an iterative process to obtain optimal solutions for the inversed problem. Such methods can achieve reasonable retrieval through these procedures.

Fundamentally, however, satellite-based estimation is highly uncertain compared with direct observations, and the complexities of cloud distributions and constitutions further increase the uncertainties in the estimation process. Thus, the procedure includes many sources of error, including the assumptions of the RTM, model parameters, solving method, and model inputs. These errors can lead to incorrect data or conclusions due to misinterpretation of a measured quantity. To appropriately use satellite-based PMW measurements, uncertainties in the estimation process must be carefully investigated and clarified in detail.

With regard to the error sources in CWC estimation using satellite-based PMW measurements, one of the biggest uncertainties is the representation of land-surface radiation, which provides necessary background information for

Manuscript received November 7, 2019; revised March 20, 2020; accepted April 20, 2020. Date of publication June 10, 2020; date of current version January 21, 2021. This work was supported by Grants-in-Aid for Scientific Research of Japan Society for the Promotion of Science (JSPS KAKENHI), Grant Numbers JP18H03800, JP19K23532 and by Japan Aerospace Exploration Agency (JAXA) commissioned research JX-PSPC-500188. (Corresponding author: Rie Seto.)

Rie Seto and Shinjiro Kanae are with the Tokyo Institute of Technology, Meguro-ku, Tokyo 152-8550, Japan (e-mail: seto.r.ac@m.titech.ac.jp; kanae@cv.titech.ac.jp).

Kentaro Aida and Toshio Koike are with the International Centre for Water Hazard and Risk Management, Tsukuba 305-8516, Japan (e-mail: aida-k677bt@pwri.go.jp; koike@icharm.org).

Color versions of one or more of the figures in this article are available online at <https://ieeexplore.ieee.org>.

Digital Object Identifier 10.1109/TGRS.2020.2996239

CWC estimation over land [10]. Because land-surface radiation has high spatial and temporal heterogeneity, it is impossible to determine its distribution from satellite observations reliably, even without the presence of clouds present. Moreover, when clouds are present over land, they can dramatically and suddenly change the land state by obstructing sunlight and sometimes providing rainfall. These changes in the land state cause changes in physical temperature and emissivity from the land surface, thus complicating the behavior of MW radiation over land in the presence of clouds. Therefore, CWC estimation techniques using satellite-based PMW measurements, such as those described above [1]–[9], are currently used mainly over oceans, while CWC data are rarely available over land [11].

However, CWC data over land have a different significance from those over the ocean due to their direct relevance to human society and regional climate, as well as to large-scale circulation. Thus, homogeneous estimation of CWC over land and ocean using satellite-based PMW measurements is desirable. Some studies have used satellite-based PMW measurements over land, thus treating the effect of land-surface radiation as a statistical error [8]. However, land-surface radiation must be confirmed intrinsically every time it is used for CWC estimation, as it can show great variation, both temporally and spatially. One method of CWC estimation that can be applied over land was developed by Seto *et al.* [12] in 2018, but its application was limited to a few cases. To optimize such methods and apply them to broad areas over land, a detailed understanding of the radiative transfer process between the land and the atmosphere is needed.

In this study, to obtain the basic information necessary to improve such methods, we investigated the characteristics of MW radiative transfer between the land and the atmosphere in the presence of clouds. MW frequencies higher than about 30 GHz are affected by CWC, and frequencies around 90 GHz are very sensitive to CWC. Most studies have addressed the radiative characteristics at these frequencies separately for clouds and the land surface, so interactions of MW radiative transfer between the land and the atmosphere in the presence of clouds have not been adequately elucidated. Therefore, this study aimed to reveal quantitatively the features and relationships of important parameters related to MW radiative transfer between land and atmosphere at 89 and 36 GHz (CWC-sensitive frequencies) in the presence of clouds by theoretical considerations and utilizing ground-based passive MW observations and RTM simulations. Finally, this study elucidates the accuracy of land emissivity representation required for the estimation of CWC over land using satellite-based PMW measurements under various CWC conditions. This study does not address MW radiative transfer within each medium (land or atmosphere) in detail, and the land cover considered in this study is limited to bare soil.

II. MW RADIATIVE TRANSFER BETWEEN THE LAND AND THE ATMOSPHERE

In this section, important equations of MW radiative transfer between the land and the atmosphere are briefly surveyed.

Using the appropriate approximations, we identify variables that must be considered when estimating CWC over land using satellite-based PMW measurements.

A. Brightness Temperature Observed via Satellite Over Land

Applying the Rayleigh–Jeans law, the radiant energy of an electromagnetic wave in the MW region can be expressed as the brightness temperature (T_B), which has the dimension of temperature. The upward brightness temperature at height r in the atmosphere can be described as follows:

$$T_B(r) = T_{B1}e^{-\tau(0,r)} + T_{Batm}(r) \quad (1)$$

where T_{B1} is the brightness temperature of the land surface, $\tau(0, r)$ is the optical depth from the land surface to height r , and $T_{Batm}(r)$ denotes the brightness temperature corresponding to radiation emitted and extinguished by the atmosphere that reaches height r .

B. MW Radiative Transfer at the Boundary Between Land and Atmosphere

At the boundary surface between the atmosphere and the land, radiation is reflected and refracted due to the large differences in the characteristics of radiative transfer of the land and the atmosphere. In this study, the canopy layer is not considered, so “land” indicates bare soil and “land surface” indicates the boundary surface between the atmosphere and the bare soil.

When the land surface is relatively smooth relative to the MW wavelength, the reflectivity of the land surface (Γ_p , where $p = h$ for horizontal polarization and $p = v$ for vertical polarization) is given in the following form [13]:

$$\Gamma_h = \left| \frac{\cos \theta - \sqrt{\epsilon_r - \sin^2 \theta}}{\cos \theta + \sqrt{\epsilon_r - \sin^2 \theta}} \right|^2 \quad (2)$$

$$\Gamma_v = \left| \frac{\epsilon_r \cos \theta - \sqrt{\epsilon_r - \sin^2 \theta}}{\epsilon_r \cos \theta + \sqrt{\epsilon_r - \sin^2 \theta}} \right|^2 \quad (3)$$

where θ is the incident angle and ϵ_r is the relative dielectric constant of soil, which is determined mainly from soil properties such as soil moisture and soil texture [14]. For a rough land surface, soil roughness must be taken into account in the estimation of Γ_p to represent surface scattering [15].

According to the conservation of energy among the incidence, reflection, and penetration of radiance, land-surface emissivity (ϵ_p) measured from the atmosphere side is described by transmissivity from land to atmosphere.

$$\epsilon_p = 1 - \Gamma_p. \quad (4)$$

C. Brightness Temperature of Land Surface

When considering radiative transfer between land and atmosphere, the land-surface radiation term (T_{B1}) includes both land-surface emission and reflection of downward radiation from the sky

$$T_{B1} = T_{B1e} + \Gamma_p T_{Bsky}. \quad (5)$$

Here, T_{Ble} is the brightness temperature corresponding to emission from the land surface, while T_{Bsky} is the brightness temperature of downward radiation from the sky.

Let T_{Bsoil} denote the brightness temperature that reaches the land surface from the interior of the soil and $T_s(r')$ denote the physical temperature of the soil at a depth of r' . Then, T_{Ble} is described as

$$T_{\text{Ble}} = \varepsilon_p T_{\text{Bsoil}} = \varepsilon_p \int_0^\infty k_e T_s(r') e^{-\tau(0,r')} dr' \quad (6)$$

where k_e is the volume extinction coefficient for that MW wavelength. When calculating radiative transfer for dry soil with a volumetric soil moisture content of less than about 10%, volume scattering cannot be neglected, and therefore, serial radiative transfer in the vertical direction within soil layers must be considered.

However, for wet soil with moisture greater than 10%, volume scattering can reasonably be neglected, as electromagnetic waves from deep in the soil are effectively attenuated. If we assume that the soil is sufficiently thick with no lower boundary and ε_r is constant and $T_s(r')$ has a constant value equal to the land-surface temperature (T_{s0}) within the soil layer where MW radiative transfer is considered, T_{Bsoil} becomes equal to T_{s0}

$$T_{\text{Bsoil}} = T_{s0}(1 - e^{-\tau(0,\infty)}) \approx T_{s0}. \quad (7)$$

If soil parameters such as $T_s(r')$ and ε_r vary with depth, the soil can be divided into several layers, in which soil parameters are reasonably constant. Then, the radiative transfer can be calculated considering reflection and refraction at the layer boundaries.

D. Important Parameters for Satellite-Based MW Cloud Estimation Over Land

Based on (1)–(6), upward brightness temperature at height r can be described as follows:

$$\begin{aligned} T_B(r) &= T_{\text{Ble}} e^{-\tau(0,r)} + T_{\text{Batm}}(r) \\ &= (\varepsilon_p T_{\text{Bsoil}} + (1 - \varepsilon_p) T_{\text{Bsky}}) e^{-\tau(0,r)} + T_{\text{Batm}}(r). \end{aligned} \quad (8)$$

Based on these considerations, we obtained three essential parameters for examining and understanding radiative transfer processes between the atmosphere and land in the presence of clouds: 1) the emissivity of the land (ε_p), which determines the reflection of downward radiation from the sky at the land surface; 2) the brightness temperature of the land surface (T_{BI}), which acts as background information; and 3) the downward brightness temperature from the sky (T_{Bsky}), which accounts for a substantial part of T_{BI} .

In actual CWC estimation procedure using satellite-based PMW measurements, the difference between the simulated brightness temperature at the top of the atmosphere ($T_B(r = r_{\text{toa}}) = T_{\text{Btoa}}$) and the satellite-observed brightness temperature (T_{Bobs}) is used to identify the best estimates by iteratively changing CWC conditions. In these procedures, land-surface radiation is usually included as constant background data for CWC estimation (accordingly, it has a constant value). However, as shown in (8), changing CWC

conditions alters the land-surface radiation due to reflection, and the factor that determines the amount of reflection is land-surface emissivity (ε_p).

Thus, for appropriate CWC estimation, T_{BI} must be calculated every time, assuming different CWC distributions (resulting in different T_{Bsky} values). Therefore, it is essential to know the instantaneous values of land-surface radiation and land emissivity, rather than statistics or error characteristics. In practical terms, it is important to clarify in advance the level of accuracy of these values required for reasonable CWC estimation.

III. RELATIONSHIP BETWEEN LAND-SURFACE RADIATION AND DISPERSION IN LAND-SURFACE EMISSIVITY

According to (4)–(6), we can formulate the relationship between changes in land-surface emissivity ($\Delta\varepsilon_p$) and land-surface radiation (ΔT_{BI})

$$\Delta T_{\text{BI}} = \Delta\varepsilon_p (T_{\text{Bsoil}} - T_{\text{Bsky}}) \approx \Delta\varepsilon_p (T_{s0} - T_{\text{Bsky}}) \quad (9)$$

where ΔT_{BI} denotes corresponding changes in T_{BI} when ε_p deviates by $\Delta\varepsilon_p$. This equation indicates that when T_{Bsoil} (or T_{s0} of a uniform soil profile) and T_{Bsky} are sufficiently similar, ΔT_{BI} becomes small even with substantial heterogeneity in ε_p . Under such conditions, changes in land emissivity may offset the changes in reflection of downward radiation, and consequently, T_{BI} will not change much. This feature has been predicted theoretically but rarely considered explicitly in previous studies or used in practical applications [8], [10].

The estimation error of T_{BI} directly affects the error in T_{Btoa} through the relationship of (1) and then propagates to the error in CWC estimation. On the other hand, the relationship between $\Delta\varepsilon_p$ and ΔT_{BI} described in (9) indicates that for estimating CWC over land from satellite-based PMW measurements, it is possible that the error in T_{BI} due to the heterogeneity of land emissivity can reasonably be neglected under certain conditions of the difference between T_{Bsoil} and T_{Bsky} .

Based on (9), if the estimation error in T_{BI} must be lower than ΔT_{BI}^D for appropriate CWC estimation, the downward radiation from the sky should be

$$T_{\text{Bsky}} > T_{\text{Bsoil}} - \frac{1}{\Delta\varepsilon_p} \Delta T_{\text{BI}}^D. \quad (10)$$

The brightness temperatures of the land surface (T_{Bsoil}) in most regions are considered to rarely exceed 315 K since the surface physical temperature rarely goes above this value, and in areas where the surface physical temperature is extremely high, soil is considerably dry [16] and we have to consider volume scattering effect, which decreases T_{Bsoil} according to (7). Therefore, if T_{Bsoil} is considered to have a maximal value within the natural range of T_{Bsoil} , for example, 315 K, the condition of T_{Bsky} for appropriate CWC estimation neglecting $\Delta\varepsilon_p$ can be described as follows:

$$T_{\text{Bsky}} > 315 - \frac{1}{\Delta\varepsilon_p} \Delta T_{\text{BI}}^D. \quad (11)$$

In the following sections, we utilize ground-based observations and model simulations to clarify the conditions for neglecting the heterogeneity of land emissivity reasonably

TABLE I
INSTRUMENTS FOR GROUND-BASED OBSERVATION

Obs. values	Observation target	Instruments
Temperature (K)	Land surface	Infrared radiative thermometer THI-700F (TASCO)
Volumetric soil moisture content (%)	Averaged in soil from surface to 10 cm depth	HD-2 Soil moisture probe TRIME-PICO32 (IMKO)
Brightness temperature (K)	Land surface and atmosphere (36 and 89 GHz, horizontal and vertical polarization)	Microwave radiometer

within the limitation of real possible land and cloud situations. Furthermore, for the case where the dispersion of emissivity cannot be reasonably ignored, we quantitatively discuss the accuracy of land emissivity representation needed to estimate CWC with adequate accuracy using satellite brightness temperature observations.

IV. GROUND-BASED OBSERVATIONS

A. Instrumentation

We carried out observations at a site located in Tsukuba, Ibaraki, Japan (36° 6' 51" N, 140° 05' 39" E). The site is about 30 m² and is covered with bare soil. The soil texture at the site is classified as silty soil. The mass ratio determined from grain-size analysis is 0.18 : 0.65 : 0.17 (clay: silt: sand).

Table I shows the observed values and instruments used. Main observation targets are the brightness temperatures of sky and land surface. The ground-based MW radiometer (GBMR) observes MW brightness temperature at four frequencies (6, 10, 36, and 89 GHz) with horizontal and vertical polarizations. This study uses measurements at 36 and 89 GHz, which are often used for CWC estimation. The GBMR is on the universal revolving table, as shown in Fig. 1. For the observation of brightness temperature of the sky, the elevation angle of the GBMR was set to 35°, in accordance with that of Advanced Microwave Scanning Radiometer (AMSR2) onboard the GCOM-W1 Satellite. For land-surface brightness temperature, the elevation angle was set to -35°. The field of view of the GBMR is about 7 m in depth and 3 m in width. It samples once per second, and the average of 100 samples is used as the observed data.

Soil moisture was measured by HD-2 Soil moisture probe at 21 different points within the GBMR footprint, and the average was used as observation data. We also check the soil moisture values using soil samples from different three points. With the sample, soil moisture is obtained as the difference between the weights of samples before and after drying it up. The soil moisture values from two methods were accordant to each other by a majority of 1%–2% in volumetric content.

A land-surface temperature is measured by an infrared radiative thermometer. We measured temperature at six different points within the footprint, and the average was used as observation data. The standard deviation of observed values is about 0.5 K.

B. Downward Brightness Temperature From the Sky

1) *Observational Conditions:* The downward brightness temperature from the sky (T_{Bsky}) was observed to determine

its range depending on water vapor conditions, the presence of clouds, and the thickness of clouds. The downward brightness temperature from our galaxy at frequencies greater than 5–10 GHz is less than 0.1 K, which is small enough to neglect compared to that from the atmosphere [17]. At these frequencies, T_{Bsky} is composed mainly of MWs emitted by water vapor, oxygen, and CWC. Some MWs emitted from the atmosphere are also attenuated by the atmosphere on the way to the ground.

We selected observation days in October and November (ON) 2018 and April 2019 when there were various weather conditions (clear sky, cloudy, and rainy) so that we could observe as wide a range of T_{Bsky} as possible. The weather of the observation days is classified based on visual inspection. The weather was judged as clear-sky condition when the cloud amount is near 0 and cloudy condition when the cloud amount is 10. We analyzed only data observed on cloudy days when rain did not fall for at least half a day after the observation time. Thus, the clouds should have contained few or no large raindrops on cloudy days. It is difficult to observe T_{Bsky} using GBMR during heavy rain, as rainfall deposited on its radome obscures accurate observation. Thus, we used T_{Bsky} observed just after it started to lightly rain as observations in the rainy conditions.

Fig. 1 shows pictures of the sky under each weather condition. Under clear-sky conditions, almost no clouds are visible, and the main contributors to T_{Bsky} are emissions from water vapor and oxygen. Around the Kanto region, where the observation site is located, the atmosphere is relatively dry in autumn and winter (approximately from October to February) compared to spring and summer (approximately from May to September). When the sky was visibly covered with clouds, as shown in the picture, conditions were considered cloudy.

2) *Observational Results:* Table II shows the minimum, maximum, and average values of observed downward brightness temperatures from the sky (T'_{Bsky} ; hereafter, variables with ' indicate observed values of the variable) at 89 GHz under each weather condition and each polarization. An individual observed value is shown in a figure in the Appendix.

Under clear-sky conditions, the values observed in April were higher than those in ON. This difference in T'_{Bsky} reflects a difference in the water vapor conditions, accounting for about 19 K.

All T'_{Bsky} values (Min., Max., and Ave.) were higher on cloudy days than those on clear-sky days. The range of T'_{Bsky} (Max.–Min.) was also wider on cloudy days than that on



Fig. 1. Pictures of the sky on the observation days of each weather condition.

 TABLE II
 OBSERVED DOWNWARD BRIGHTNESS TEMPERATURE FROM THE SKY

Weather	Obs. day	V/H	T _b (K)		
			Min.	Max.	Ave.
Clear-sky	ON	V	52.4	88.3	72.6
		H	53.2	89.1	73.3
	April	V	78.0	103.5	91.4
		H	78.7	103.6	91.6
Cloudy	ON & April	V	112.6	214.6	153.2
		H	113.0	214.5	153.1
Rainy	ON & April	V	168.5	226.2	189.6
		H	168.5	226.0	189.5

clear-sky days. T'_{Bsky} varied relatively strongly depending on the CWC distribution. These results indicate that both the effect of CWC on T_{Bsky} and the sensitivity of CWC to T_{Bsky} are greater than the effects of atmospheric (mainly water vapor) conditions.

During light rain, T'_{Bsky} values were higher than about 170 K, and the maximum value was 226.2 K. Thus, raindrops contributed to increased downward radiation. The difference due to polarization was very small for all observations in all weather conditions.

These results indicate that the presence of clouds can increase T'_{Bsky} by 2.5 times. When a large amount of rain particles are present in the clouds, T'_{Bsky} increases more than threefold. Because emissions increase as the amount

of precipitation increases, T_{Bsky} is likely to increase further during heavy rain. T_{Bsky} during heavy rain was examined using simulations, as described in the next section.

At 36 GHz, the characteristics of T'_{Bsky} were similar overall to those at 89 GHz (see the Appendix for individual data), with the lowest values on clear-sky days and the highest on cloudy and rainy days. The maximum value of measurements was about 100 K, and the average values were 38, 64, and 78 K on clear-sky, cloudy, and rainy days, respectively. These values are less than half of those obtained at 89 GHz. Although sensitivity to CWC was small, a positive relationship was observed. Differences related to polarization were very small as with 89 GHz.

C. Emissivity and Brightness Temperature of the Land Surface

1) *Observational Conditions:* Next, we conducted observations to investigate the behavior and realistic range of the brightness temperature and the emissivity of the land surface under various soil-moisture conditions. Land emissivity is most strongly affected by soil moisture [18], which changes readily in the presence of clouds or precipitation. Thus, in this study, we express the temporal heterogeneity of land emissivity by changing soil-moisture conditions. We gradually changed soil moisture with step-by-step watering during the observation. We agitated the soil with a cultivator and leveled it with a brush after each watering so that the moisture of the surface soil layer, in which 36- and 89-GHz MWs can penetrate (penetration depths at these frequencies are less than a few centimeters), would be uniform. As a result, soil moisture varied from 18.5% to 30.7% at intervals of about 2% in terms of volumetric soil moisture content (Mv). The averaged standard deviation of Mv was 1.72%.

Based on (5), T_{Bl} includes land-surface emission (T_{Ble}) and reflection of the downward brightness temperature of the sky ($\Gamma_p T_{\text{Bsky}}$), but GBMR cannot observe these values separately. Therefore, we cannot directly observe land emissivity (ε_p), which must instead be calculated from observations by removing the contribution of T_{Bsky} . According to (6), the observed value of land emissivity (ε'_p) is expressed as

$$\varepsilon'_p = (T'_{\text{Bl}} - T'_{\text{Bsky}})/(T'_{\text{Bsoil}} - T'_{\text{Bsky}}). \quad (12)$$

In this equation, T'_{Bsoil} cannot also be directly measured. Thus, we have to estimate the appropriate value for it. Basically, in the thermodynamically equilibrium state, we can assume that the profile of soil parameters such as $T_s(r')$ and ε_r is reasonably constant within the soil layer considered so that at the beginning of observation before watering, T'_{Bsoil} is nearly identical to the observed land-surface physical temperature (T'_{s0}) based on (7). After the manual increase of Mv over a relatively short time (time is less than 20 min from watering to measuring the brightness temperature within each step), however, T'_{Bsoil} values that are calculated assuming a uniform soil profile appeared to be underestimated because the physical soil temperature profile within the soil layer is not uniform due to the sudden decrease in T'_{s0} . On the other hand, because the heat capacities of soil in target moisture conditions are sufficiently low, the physical soil temperature profile under the surface layer was not so much changed due to watering. Thus, the effect of watering on radiation from the interior of the soil is assumed to be small [17], [19]. Therefore, we used surface temperature before watering ($T'_{s0\text{bw}}$) as T'_{Bsoil} of all steps even after watering. Then, land emissivity (ε'_p) can be calculated as follows:

$$\varepsilon'_p \approx (T'_{\text{Bl}} - T'_{\text{Bsky}})/(T'_{s0\text{bw}} - T'_{\text{Bsky}}). \quad (13)$$

Hereafter, we use the ε'_p calculated in the form of (13) as observations of land emissivity. Here, ε'_p includes the effect of surface scattering, as T'_{Bl} in (13) is the actual value.

We chose a clear-sky day, when the effect of T'_{Bsky} on T'_{Bl} was weaker.

2) *Observational Results*: Fig. 2 depicts the response of ε'_p to changing Mv and $T'_{\text{Bsoil}} (\approx T'_{s0\text{bw}})$ for 89- and 36-GHz data based on (13). As discussed in the previous section, we used T'_{s0} before watering ($T'_{s0\text{bw}}$) as T'_{Bsoil} for observations with all Mv conditions. Error bars indicate observational errors, which are estimated on the basis of error propagation approach using each standard deviation of observed variables (Appendix B).

For 89-GHz data, the results of ε'_p show ranges of variation of 0.866–0.917 and 0.897–0.940, with varying widths of about 0.04 and 0.05, for horizontal and vertical polarizations, respectively. In terms of land emissivity, a clear difference was observed between polarizations. ε'_p was lower for horizontal polarization than that for vertical polarization under all Mv conditions. The results show that ε'_p decreased as Mv increased, which is expected by (2), (3), and the relationship between relative dielectric constant (ε_r) and Mv (relative dielectric constant ε_r increases with Mv [20]). Observational errors that are shown by error bars are sufficiently small so that the errors have little effect on the characteristics we can recognize from the results.

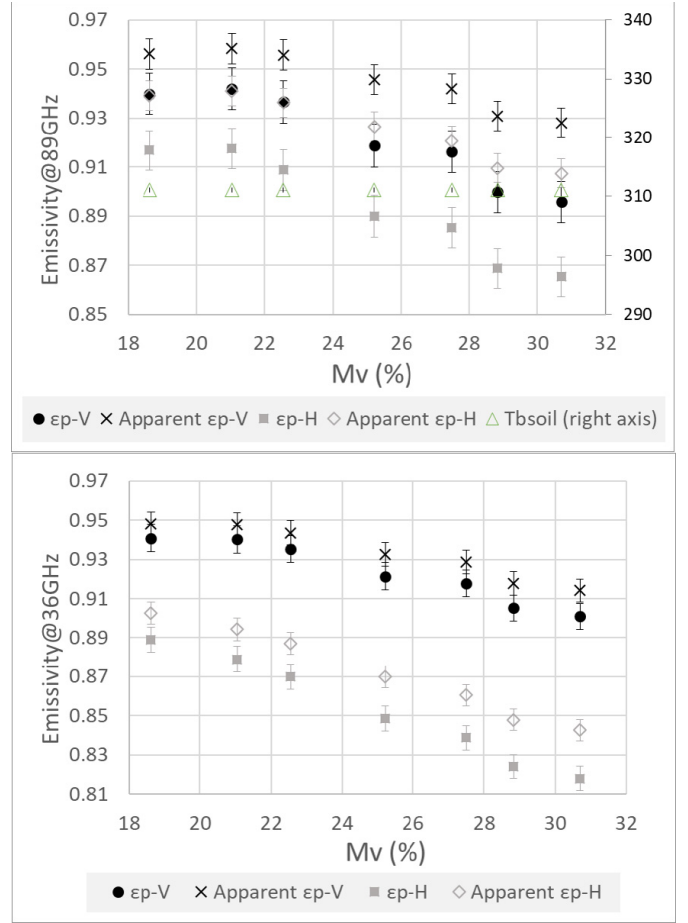


Fig. 2. Change in corrected land emissivity with different soil moisture conditions observed at (Top) 89 and (Bottom) 36 GHz, and land-surface physical temperature before watering (top).

Fig. 2 also shows “apparent emissivity,” which was calculated simply by dividing T'_{Bl} by T'_{s0} , and therefore includes the contribution of reflected downward radiation from the sky. Apparent emissivity was overestimated by about 0.03 and 0.04 for vertical and horizontal polarizations, respectively. Even on a clear-sky day, the error was comparable to the amount of change in emissivity due to Mv conditions. Therefore, it is important that investigations of ε_p using GBMR observations consider the effects of reflection carefully.

Emissivity was generally lower at 36 GHz than that at 89 GHz, but its response to changes in Mv was similar. A relatively large difference was observed between the two polarizations. For horizontal polarization, emissivity at 36 GHz was more sensitive to Mv change, with a varying width of about 0.07. Because T'_{Bsky} was much lower at 36 GHz than that at 89 GHz, the error in emissivity due to T'_{Bsky} (the difference between ε'_p and apparent ε'_p) was smaller at 36 GHz than that at 89 GHz. However, it is still largely overestimated by about 0.025.

Fig. 3 shows the observed brightness temperatures of the land surface (T'_{Bl}) and the brightness temperatures corresponding to emission from the land surface (T'_{Ble}), which was calculated as follows:

$$T'_{\text{Ble}} = \varepsilon'_p T'_{\text{Bsoil}} \approx \varepsilon'_p T'_{s0}. \quad (14)$$

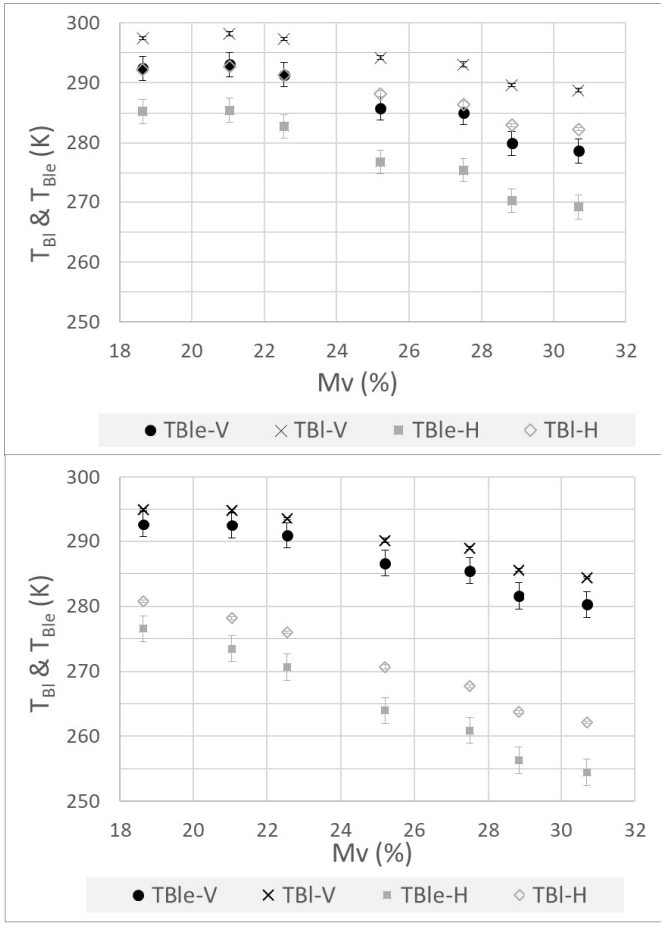


Fig. 3. Change in brightness temperatures corresponding to land emission and land-surface radiation with different soil moisture conditions observed at 89 (upper) and 36 (lower) GHz.

T'_{BI} was greater than T'_{Ble} by about 5–10 K. As for the difference between land emissivity and apparent land emissivity (Fig. 2), this difference ($T'_{BI} - T'_{Ble}$) was comparable to the amount of change in land radiation due to Mv conditions or ϵ_p conditions, and also, it is much larger than observational errors. This indicates the significance of partitioning of emission and reflection in land radiation for appropriate observations and investigations of radiative properties of land surface using GBMR if clouds exist over the land.

D. Brightness Temperature of the Land Surface in the Presence of Clouds

1) *Observational Conditions*: In this section, we explore the response of the brightness temperature of the land surface (T_{BI}) to various soil-moisture (according, land-surface emissivity) conditions in the presence of clouds of varying thickness (that is, varying LWP values). Through this observation, we aimed to check the possibility that we can neglect the heterogeneity of land-surface emissivity in CWC estimation as discussed in Section III even within the actual conditions. We cannot determine the exact value of T_{BI} corresponding to various LWP conditions, as no LWP data are available from the time of observation because T_{BI} can be observed only under

conditions of no or light rain. However, the pseudo-observed term (T'_{BI}) can be obtained under certain cloud conditions by assuming the appropriate downward brightness temperature from the sky (T'_{Bsky}) based on observations and adding the effect of reflection to T'_{Ble} using the value of ϵ'_p obtained from observations.

We considered five cloud and rain conditions and the corresponding value of T'_{Bsky} : first, thin clouds without rain, where $T'_{Bsky} = 120$ and 60 K for 89 and 36 GHz, respectively; second, relatively thick clouds without rain, where $T'_{Bsky} = 160$ and 80 K; third, clouds with light rain, where $T'_{Bsky} = 200$ and 100 K; fourth, clouds with relatively heavy rain, where $T'_{Bsky} = 280$ and 160 K; and fifth, clouds with extremely heavy rain, where $T'_{Bsky} = 300$ and 250 K for 89 and 36 GHz, respectively. We determined the value of T'_{Bsky} based on the ground-based observations for cloudy and light-rain conditions, and for heavy rain conditions, we referred to the tendency of ground-based observation and simulation results (see Section V). The last settings approximately assume the possible maximum value of T'_{Bsky} with extreme heavy rain in order to check the possibility of neglect of $\Delta\epsilon_p$ within the natural conditions.

2) *Observational Results*: Fig. 4 shows the pseudo-observations of T'_{BI} calculated using the ϵ'_p values shown in Fig. 2. For both 89- and 36-GHz data, T'_{BI} reaches its maximum value when clouds are thick and is lowest with thin clouds. As shown in Table II, the values of T'_{Bsky} are similar for both polarizations, thus meaning that larger T'_{Bsky} results in a smaller difference in T'_{BI} between polarizations.

Furthermore, it is notable that the higher the T'_{Bsky} , the smaller the change of T'_{BI} with Mv conditions is. When T'_{Bsky} is 280 and 300 K for 89 GHz and 250 K for 36 GHz, T'_{BI} is nearly constant regardless of Mv conditions. For example, under the thin-cloud condition ($T'_{Bsky} = 120$), T'_{BI} ranges from 285 to 295 K, while under the extremely heavy rain condition ($T'_{Bsky} = 300$), it ranges from 309 to 310 K for horizontal polarization of 89 GHz. For 36 GHz, under the extremely heavy rain condition ($T'_{Bsky} = 250$), T'_{BI} ranges from 305 to 307.5 K.

These results show that the dispersion of land-surface radiation ($\Delta T'_{BI}$) corresponding to a realistic variation of ϵ'_p becomes sufficiently small when T'_{Bsky} is high about 280 K for 89 GHz and 250 K for 36 GHz. This means that observational results also indicate that we can neglect the heterogeneity of land-surface emissivity even within the real situation if we can select sufficiently thick cloud conditions.

For 89 GHz, the dispersion of land emissivity can be greater than 0.05 for both frequencies based on the results of ground-based observations described above (Fig. 2). Then, according to (11), the condition of T_{Bsky} is given in the following form:

$$T_{Bsky} > 315 - 20\Delta T_{BI}^D. \quad (15)$$

For 36-GHz data, the dispersion of land emissivity can be about 0.07 for both frequencies based on the results of ground-based observations (Fig. 2). Similar to 89 GHz, the condition of T_{Bsky} can be described as follows:

$$T_{Bsky} > 315 - 15\Delta T_{BI}^D. \quad (16)$$

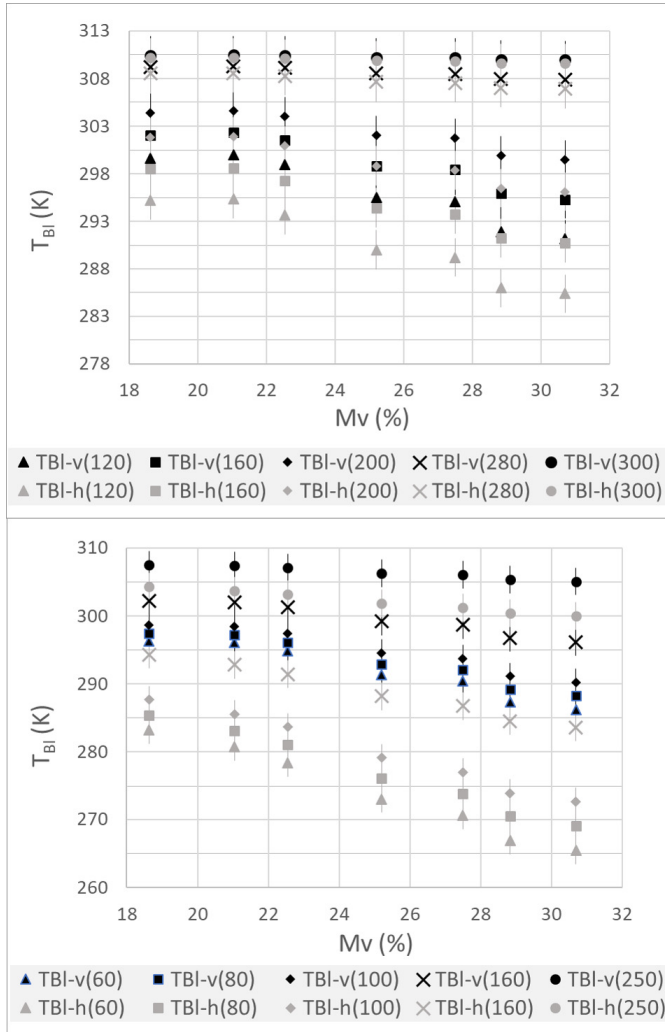


Fig. 4. Change in brightness temperature of land-surface radiation with different soil moisture conditions under the presence of clouds observed at 89 (upper) and 36 (lower) GHz.

Because T_{Bsky} at 36 GHz is relatively low than 89-GHz data and dispersion of emissivity is larger than that of 89 GHz, more limited conditions are expected to be needed for neglecting heterogeneity in land-surface emissivity for 36 GHz. Therefore, to use 36-GHz MW data for CWC estimation, land emissivity is appeared to be represented with relatively high accuracy.

By determining the desirable error value for T_{BI} (ΔT_{BI}^D), these thresholds can be determined using only the value of T_{Bsky} , (or accordingly, that of the LWP). Based on this consideration, in the following section, we determine the threshold value of T_{Bsky} and the corresponding LWP value using model simulations. Moreover, we clarify the accuracy of T_{BI} representation and that of heterogeneity in land-surface emissivity (ϵ_p) needed for reasonable satellite-based CWC estimation over land, based on a case where the difference between T_{Bsoil} (or T_g) and T_{Bsky} is larger than the threshold.

Then, we examined the threshold value of the difference between T_{Bsoil} and T_{Bsky} (accordingly, the LWP value) for estimation of CWC without accounting for the heterogeneity of ϵ_p .

TABLE III
CLOUD TOP AND BOTTOM HEIGHT SETTINGS

Indication	Cloud top (m)	Cloud bottom (m)
CTB1015	10000	1500
CTB1030	10000	3000
CTB1050	10000	5000
CTB1080	10000	8000
CTB515	5000	1500
CTB530	5000	3000
CTB315	3000	1500

V. SIMULATION

In this section, we examine the threshold of T_{Bsky} and the corresponding LWP value needed for accurate estimation of CWC while neglecting the heterogeneity of ϵ_p using model simulations. We also used model simulations to calculate the upward brightness temperatures at the top of the atmosphere (T_{Btoa}), along with the corresponding LWP values and several surface conditions, to determine the sensitivity of T_{Btoa} to LWP values and the appropriate value of ΔT_{BI}^D .

Finally, a threshold value is proposed from satellite-based PMW brightness temperature data. This threshold can be used for the classification of measurements to handle them prior to full analysis. We also clarify the required accuracies of representation of T_{BI} and ϵ_p for T_{Bsky} values below the threshold. In simulations, we also consider the effect of cloud-bottom height conditions.

A. Radiative Transfer Model

To calculate downward brightness temperature from the sky (T_{Bsky}) and upward brightness temperature at the top of the atmosphere (T_{Btoa}), we used an RTM based on the four-stream fast model reported in [21], which employs the four-stream approximation method for radiative flux calculation. We set the zenith angle for radiative transfer calculation to 55° , which is the same as GBMR. The inputs to this model include atmospheric profiles, CWC distributions, and lower boundary conditions such as land-surface radiation and land emissivity (reflectivity).

In the four-stream fast model, we conducted simulations with several sets of cloud top and bottom heights. The settings and experimental names are shown in Table III. (Hereafter, simulations using these settings are called using "indication" in Table III.) The size distribution of cloud particles was assumed to follow a gamma distribution, and only liquid water particles were considered.

For the profiles of atmospheric factors, such as temperature and water vapor, outputs from the atmospheric model were used. The output profiles were modified to consider the temperature increase caused by latent heat and water vapor

saturation within the cloud layer corresponding to the CWC distribution. An example of the profiles used is shown in Fig. 10. The vertical distribution of CWC against geophysical height was assumed to be parabolic.

We simulated T_{BI} under a soil moisture range including extremely dry and wet conditions in the presence of various cloud levels. Land emissivity and land-surface brightness temperatures were calculated using land RTM with the advanced integral equation model originally developed by Chen *et al.* [22], which reflects the effect of surface scattering and can be applied to high-frequency MW data [15]. ϵ_r was calculated from soil moisture and soil texture based on Dobson's formula [14]. Soil porosity was set to 0.35, the standard deviation of soil roughness (h_v) was 0.5, and the autocorrelation length was $2.5h_v - 0.21$.

B. Brightness Temperatures Downward From the Sky and Upward at the Top of the Atmosphere

1) *Simulation Results:* We conducted simulations under several LWP conditions for CTB1015, CTB1030, CTB1050, CTB1080, CTB515, CTB530, and CTB315. LWP was set to the following 16 values: 0.2, 0.4, 0.6, 0.8, 1, 1.2, 1.4, 1.6, 1.8, 2, 3, 4, 5, 6, 7, or 8 kg/m² (hereafter, these simulations are referred to as Wc0.2–Wc8).

Simulated T_{Bsky} and T_{Btoa} values for vertical polarization are shown in Figs 5 and 6, respectively, (results of horizontal polarization were nearly identical to those of vertical polarization and are not shown) for both 89- and 36-GHz data.

For 89-GHz data, the range of T_{Bsky} extended from around 200 to 290 K. The simulation results show that T_{Bsky} increases as LWP values increase, as recognized in the ground-based observation results. As cloud-bottom height becomes lower, T_{Bsky} increases. The difference in T_{Bsky} between CTB1050 and CTB1015 is 4–10 K, while that between CTB1080 and CTB1050 is around 5–12 K. On the other hand, cloud top heights do not much affect on T_{Bsky} . The rate of increase of T_{Bsky} gradually decreases with increasing LWP values. When the LWP value is greater than about 2 kg/m², the change in T_{Bsky} due to cloud-bottom height is greater than that due to a change in the LWP value of 1 kg/m².

For 36-GHz data, the differences in T_{Bsky} among cloud-bottom height conditions are smaller than those for 89-GHz data. Unlike for 89 GHz, the rate of change of T_{Bsky} with LWP increase does not become small with a large LWP.

As shown in Fig. 6, for 89-GHz data, the sensitivity of T_{Btoa} to the LWP value decreases as LWP values increase, while sensitivity is high with LWP values of less than 2 kg/m². For 36-GHz data, the sensitivity of T_{Btoa} to LWP values is generally higher than that for 89-GHz data even if LWP is more than 2 kg/m². The sensitivities do not differ markedly among cloud-bottom conditions at either 89 or 36 GHz. On the other hand, T_{Btoa} is largely affected by cloud top height. Especially, for 36 GHz, there is a little sensitivity to LWP values if the cloud top height is lower than 5 km. This means that to estimate CWC for these clouds, the utilization of the higher frequency MW is appropriate.

2) *Threshold Determination (LWP):* As shown in Fig. 6, if cloud top is low (~ 5 km), the sensitivity of T_{Btoa} to

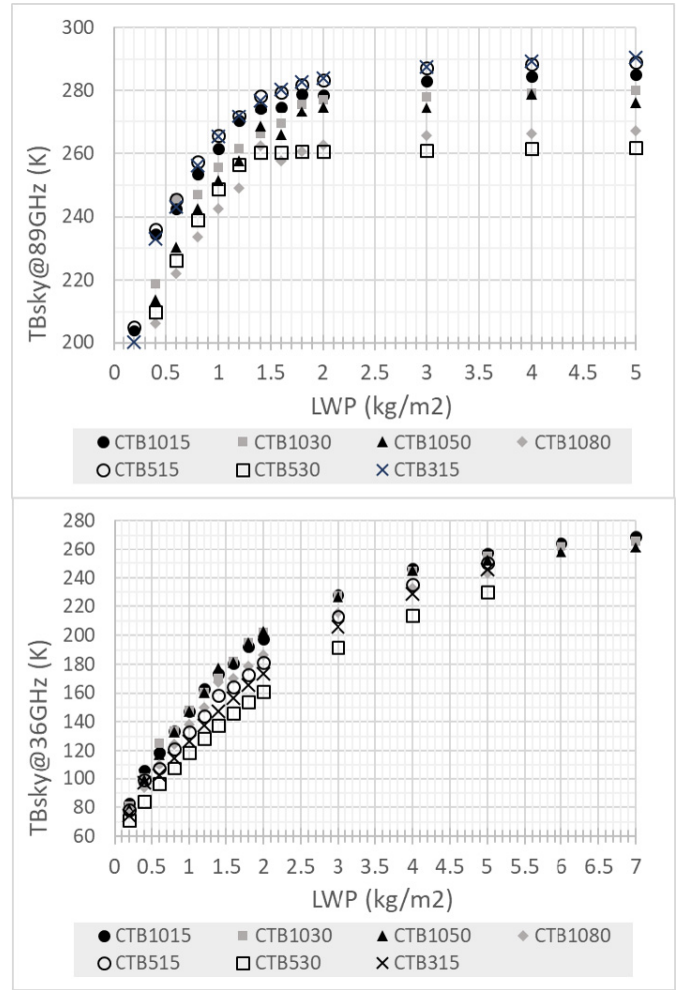


Fig. 5. Difference in downward brightness temperature of the sky under different cloud water path and cloud-bottom height conditions.

LWP is very small so that the smaller error of T_{Btoa} is required. However, (15) and (16) suggest that the threshold of T_{Bsky} becomes substantially large if acceptable error of T_{Btoa} (accordingly, ΔT_{BI}^D) is small, and in such conditions, LWP is expected to be quite large and the cloud top height is high. Therefore, it is expected that the threshold conditions become high cloud top, low cloud bottom, and large LWP. Thus, to determine the value of ΔT_{BI}^D , we basically use the results from CTB1015, CTB1030, and CTB1015, assuming conditions of high cloud top (~ 10 km), low cloud bottom (lower than 5 km), and large LWP ($LWP > 1$ kg/m²).

According to (1), the upper limit of desirable error in T_{BI} (ΔT_{BI}^D) can be the same level with the acceptable error of T_{Btoa} . For 89-GHz data, based on the results of T_{Btoa} simulation (CTB1015, CTB1030, and CTB1015 in Fig. 6) and those of a sensitivity test to determine the uncertainties of CWC estimation using satellite-based PMW conducted previously [12], ΔT_{BI}^D is estimated to be less than 3 K for LWP values of less than 2 kg/m² and 2 K when LWP values are greater than 2 kg/m² for CWC estimation (with such an error of T_{Btoa} , estimation error in LWP is 10%–20%).

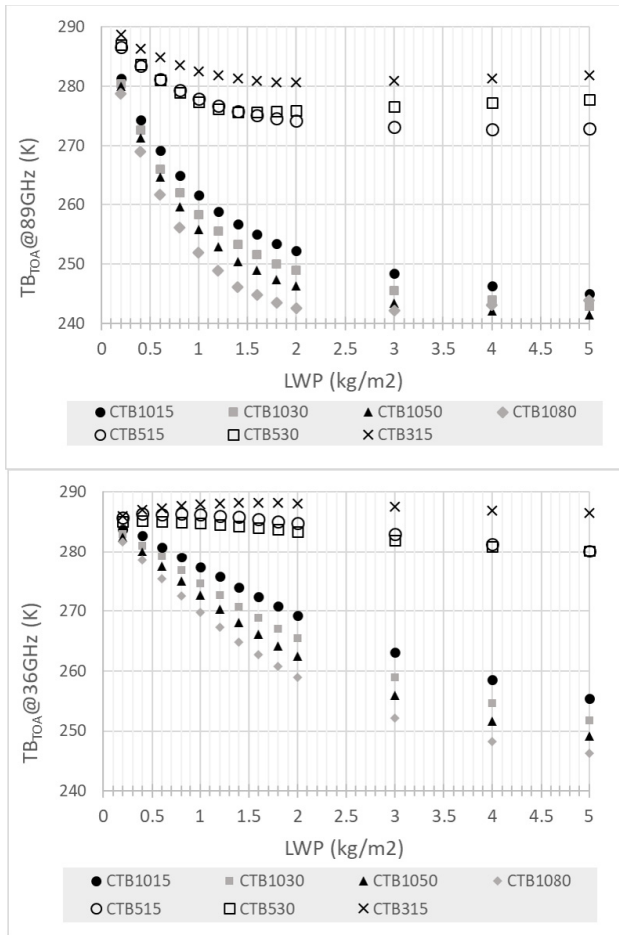


Fig. 6. Change in simulated brightness temperature at the top of atmosphere with different cloud water paths simulated at 89 (upper) and 36 (lower) GHz.

Then, for LWP values of less than 2 kg/m^2 , using (15), the threshold of T_{Bsky} is 255 K. From the results shown in Fig. 5, whenever the LWP value is higher than 1.6 kg/m^2 , T_{Bsky} is greater than 255 K.

For LWP values of more than 2 kg/m^2 , ΔT_{BI} is required to be below 2 K, and T_{Bsky} should exceed 275 K from (15). This condition is automatically satisfied with LWP more than 2 kg/m^2 , as shown in Fig. 5. If the cloud layer is thin (CTB530 and CTB310) and the LWP value is greater than 2 kg/m^2 , ΔT_{BI} increases. But in practical terms, clouds with LWP values greater than 2 kg/m^2 are expected to produce rain, and most of these clouds have a thicker cloud layer.

Accordingly, in conjunction with above discussions, if the LWP value of the target cloud exceeds 1.6 kg/m^2 , ΔT_{BI} can be considered small ($\lesssim 3 \text{ K}$). Under such conditions, the heterogeneity of land-surface radiation (T_{BI}) due to the dispersion of land emissivity ($\Delta \varepsilon_p$) can be neglected in the estimation of CWC from satellite-based PMW measurements.

For 36 GHz, the sensitivity of T_{Btoa} to LWP values is greater than that for 89 GHz, as shown in Fig. 6. Based on similar considerations, for 36-GHz data, ΔT_{BI}^D should be less than 4 K for appropriate CWC estimation from LWP values under all cloud-bottom conditions. To satisfy this requirement, T_{Bsky} must be larger than 255 K using (16), and, accordingly, the LWP value must be greater than 5 kg/m^2 .

Finally, we can reasonably determine that the threshold value of LWP that must be met to neglect the heterogeneity of ε_p is 1.6 and 5 kg/m^2 for 89- and 36-GHz data, respectively

$$\text{LWP} \geq \begin{cases} 1.6 \text{ kg/m}^2 (89 \text{ GHz}) \\ 5 \text{ kg/m}^2 (36 \text{ GHz}) \end{cases} \quad (17)$$

Because T_{Bsky} is much lower at 36 GHz than at 89 GHz, high LWP values are needed to neglect the dispersion due to land emissivity. In this section, we expected that the threshold of LWP is sufficiently large and determined ΔT_{BI}^D assuming only thick cloud conditions. From the above results, we confirm that the determined threshold of LWP is large enough. Since, for these clouds with large LWP, low cloud-top and high cloud-bottom conditions are unrealistic, it is not necessary to consider these cases.

3) *Threshold Determination (T_{Bobs}):* Thresholds in LWP values are inconvenient, as LWP values are unknown prior to the estimation of CWC. To determine the threshold using satellite measurements at the stage before processing, we propose criteria using satellite observations of brightness temperature.

Based on the simulation results of T_{Btoa} (Fig. 6), to satisfy the condition that the LWP value is greater than the threshold, the criteria can be expressed as follows:

$$T_{\text{Bobs}} < 245 \text{ K}. \quad (18)$$

This criterion can be applied to both 89- and 36-GHz data. The criteria are not necessarily the same for both frequencies, but they are conveniently similar. Under conditions of T_{Bobs} lower than 245 K, LWP values are considered to be greater than 1.6 and 5 kg/m^2 for most land and cloud conditions for 89 and 36 GHz, respectively. We also identified the effects of errors in land-surface temperatures on this criterion by conducting simulations using various land-surface temperature conditions (not shown) and found that 245 K can be used when the land-surface temperature is lower than 315 K and higher than 275 K, which includes almost all land-surface conditions. The order of the polarization difference is also negligible ($\sim 0.05 \text{ K}$) in the range of LWP corresponding to the threshold value of T_{Bobs} .

Furthermore, although we did not deal with ice particles in the simulations, (18) is thought to be applied even if ice particles exist in the upper part of clouds. This is because the land-surface radiation is larger than cloud radiation and the scattering by ice particles reflects upwelling radiation back to the land surface. Therefore, cloud ice particles over land even decrease the upward brightness temperature at the top of the atmosphere and increase the downward radiation from the sky. The existence of cloud ice particles acts in the direction of being able to neglect the variation of land-surface emissivity and in the direction of lowering satellite observation. Thus, we believe that the threshold from the results of this article is not affected. This feature is unique for conditions over land.

C. Brightness Temperature of the Land Surface

In this section, we examine the required accuracies of representation of ε_p for the case where T_{Bsky} values are

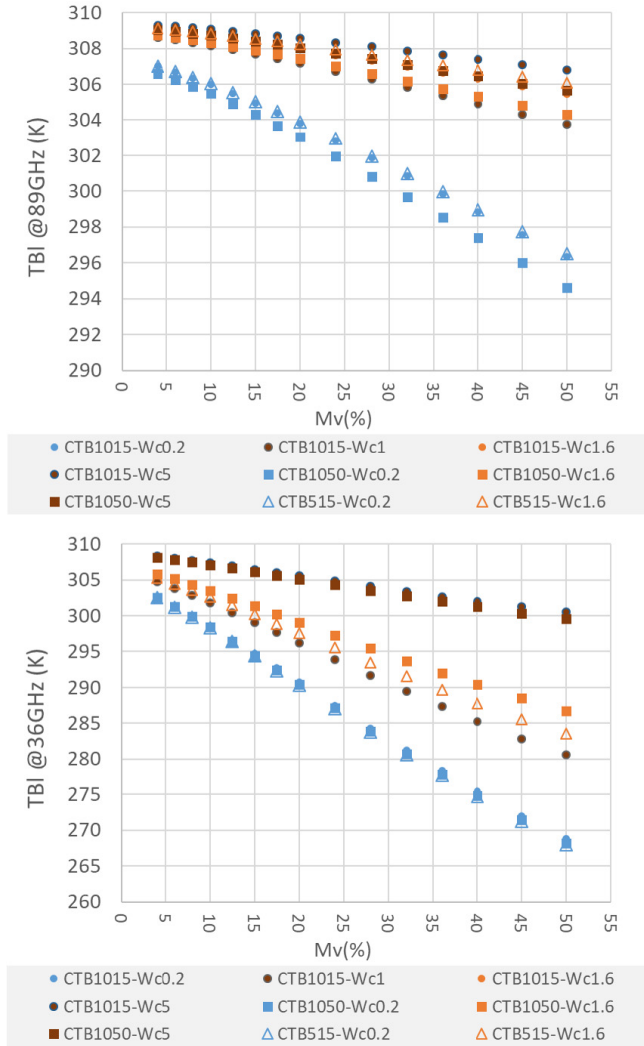


Fig. 7. Change in simulated brightness temperature of land-surface radiation with different soil moisture conditions under the presence of clouds simulated at 89 (upper) and 36 (lower) GHz.

below the threshold and the dispersion of emissivity cannot be reasonably ignored. We conducted simulations under various 19 Mv conditions (Mv is 1%, 2%, 4%, 6%, 8%, 10%, 12.5%, 15%, 17.5%, 20%, 24%, 28%, 32%, 36%, 40%, 45%, 50%, 55%, 60%, respectively) for each simulation using different cloud-bottom height and LWP values, as described above. The surface temperature was set to 310 K.

The calculated brightness temperatures corresponding to land emissions show similar features to those based on ground observations. The decreasing trend in emissions with increasing Mv is the same as that from ground-based observations (Fig. 11).

Fig. 7 depicts the results for the brightness temperature of the land surface, which includes the reflected brightness temperature of the sky for various LWP values and cloud-bottom conditions. From these results, we can confirm that the same trend was found as that from observations; that is, with high LWP values, the amount of T_{BI} variation due to Mv was small.

Under practical land-surface conditions, Mv can be considered to fall in the range 10%–40%. Fig. 8 shows contour diagrams of the difference in T_{BI} with Mv values of 10%

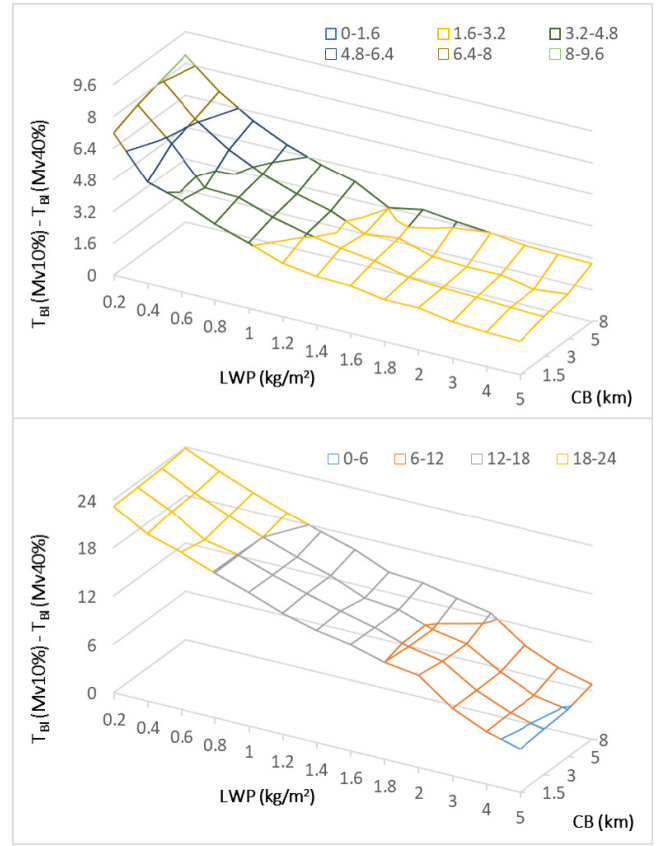


Fig. 8. Contour diagram of the difference in T_{BI} between with Mv of 10% and 40% as a function of LWP and cloud-bottom height.

and 40% as a function of LWP values and cloud-bottom height. The difference in T_{BI} is less than about 3 K when the LWP value is greater than 1.6 kg/m^2 at 89 GHz. This finding supports the validity of threshold determination for LWP values in (17).

For 36-GHz data, the difference in T_{BI} is about 5 K even with LWP values greater than 5 kg/m^2 at 36 GHz. An error was slightly greater than it was expected to be. The reason is supposed to be that in our soil RTM, the dispersion of ε_p due to Mv variation was greater (about 0.11) for the 36-GHz data than that observed with GBMR. As noted above, the dispersion under real-world conditions is about 0.07, and the error is expected to decrease to a level that satisfies the condition.

On the other hand, for LWP values lower than 1.6 kg/m^2 or a cloud-bottom height of 8000 m observed at 89 GHz, T_{Bsky} was small. In this case, the representation of ε_p must be much accurate to restrict ΔT_{BI} to sufficiently small values (less than 3 K) according to (11) as follows:

$$\Delta \varepsilon_p < \frac{\Delta T_{BI}^D}{315 - T_{Bsky}}. \quad (19)$$

Considering the range of T'_{Bsky} on cloudy days ($\sim 115 \text{ K}$ at the minimum as shown in Table II), restricting ΔT_{BI} to less than 3 K under these conditions necessitates the land emissivity having an error of less than 0.015 for 89-GHz data. Moreover, to attain this accuracy, the error of volumetric soil moisture content representation must be less than 5%–6%, considering the sensitivity of ε_p to Mv (Fig. 2).

Similarly, for 36-GHz data with LWP values lower than 5 kg/m^2 (which includes most real cases, except under heavy rain conditions), T'_{Bsky} is about 50 at minimum. To restrict ΔT_{BI} to less than 4 K, land emissivity must have an error of less than 0.015 together with a volumetric soil-moisture content of less than 5%–6%.

From these results and discussions, we found that we can reduce the calculation cost or effort needed to represent T_{BI} accurately for CWC estimation over land, especially under rainy conditions, by using 89-GHz MW data. However, for most cases without precipitation and when using only 36-GHz data, CWC estimation using satellite-based PMW measurements must be undertaken with very careful consideration of land-surface radiation and land emissivity.

VI. CONCLUSION

One of the main obstacles to accurate estimation of CWC over land is high uncertainties in radiation from the land surface. A large part of dispersion of land-surface radiation arises from the high spatial and temporal heterogeneities of land emissivity (ϵ_p). However, cloud itself also has an influence on land-surface radiation through providing downward radiation, a quite part of which is reflected by land surface back to the sky, and through altering land conditions, accordingly land emissivity (ϵ_p), by raining and intercepting the sunlight. Thus, it is important to understand the characteristics of MW transfer between the land and the atmosphere in the presence of clouds in detail, and the extent of influence of uncertainties in land emissivity representation on CWC estimation must be carefully investigated and clarified quantitatively for reliable estimation.

This study theoretically considered and clarified the important parameters related to MW transfer between atmosphere and land and the relationships of their dispersions. Through the consideration, it is indicated that there is a possibility that the dispersion in the land-surface emissivity can be reasonably ignored under appropriate conditions.

Then, we utilized ground-based PMW observations and model simulations to ascertain what condition is needed to reasonably neglect the heterogeneity of land emissivity and determine quantitatively basic information about the accuracy of land emissivity representation needed for adequate estimation of CWC if the conditions are not met.

Using GBMR data and theoretical considerations based on radiative transfer equations, we found that reflection of the downward brightness temperature from the sky ($\Gamma_p T_{\text{Bsky}}$) can contribute to mitigating the effects of land emissivity dispersion if T_{Bsky} is sufficiently high compared to the brightness temperature that reaches the land surface from the interior of the soil (T_{Bsoil}). Then, we used model simulations to determine the threshold values of T_{Bsky} and LWP for appropriate estimation without consideration of the heterogeneity of ϵ_p .

Our investigation revealed that the threshold values of T_{Bsky} and LWP needed to neglect the heterogeneity of ϵ_p are 255 K and 1.6 kg/m^2 for 89-GHz data and 255 K and 5 kg/m^2 for 36-GHz data, respectively. To determine the threshold from satellite measurements prior to data processing, we propose the use of a threshold based on brightness temperatures observed

by satellites, T_{Bobs} . When T_{Bobs} is less than 245 K, the T_{Bsky} and LWP thresholds given above for both 89- and 36-GHz data are met.

When T_{Bsky} and LWP are below their thresholds, dispersion of radiation from the land surface becomes too great for a reasonable estimation of CWC without accounting for the effect of dispersion related to land emissivity. Under these conditions, land emissivity should be represented with an error of less than 0.015 for both 89- and 36-GHz data. To obtain this accuracy, the error in volumetric soil moisture content representation must be less than 5%–6%.

This article does not account for the inhomogeneity of cloud within the footprint. The threshold obtained is “ $T_{\text{Bobs}} < 245 \text{ K}$,” so under this situation, comparably substantial precipitation should be occurring. Hence, cloud system is developed, and in a footprint of several kilometers, the distribution of clouds can be thought of as homogenous. On the other hand, when T_{Bobs} is larger than the threshold to a certain extent, the clouds may possibly be thin and distributed inhomogeneous. In this case, the LWP estimated from the satellite is the averaged value in the footprint with several kilometers width. In addition, in order to improve the accuracy of LWP estimation over land in such case, we have to appropriately represent the spatiotemporal variation of land-surface radiation from model and observation, as in [12], and mitigate the uncertainty.

The results of this study provide basic information about the MW radiative transfer process between the land and the atmosphere in the existence of clouds as well as CWC estimation over land using satellite-based PMW measurements. In particular, for estimation of CWC for rain clouds using 89-GHz data, the radiative conditions of the land surface can be accurately represented without great cost. Nevertheless, for nonprecipitating clouds and algorithms using only low-frequency MW (around 36 GHz) data, the heterogeneity of land radiation and emissivity must be taken into account, as these factors can introduce large errors into CWC estimation.

APPENDIX

A. Downward Brightness Temperature From the Sky

Fig. 9 shows T'_{Bsky} at 89 and 36 GHz. Observation numbers 1–10 in Fig. 9 indicate observations conducted on different clear-sky days in ON, while observations 11–20 were collected on April 23. Observation numbers 1–10 in Fig. 9 indicate observations conducted on different clear-sky days in ON, and 11–20 were collected on April 23.

For 89-GHz data, T'_{Bsky} values in ON ranged from 52.4 to 88.3 K with an average value of 72.6 K for vertical polarization and from 53.2 to 89.1 K with an average value of 73.3 K for horizontal polarization. Observed values were higher on April 23 than those in ON, ranging from 78.0 to 103.5 K with an average value of 91.4 K for vertical polarization and from 78.7 to 103.6 K with an average value of 91.6 K for horizontal polarization.

For cloudy conditions, observation numbers 1–7 in Fig. 9 indicate observations on various cloudy days in ON, and 8–15 indicate observations on April 24. The average values

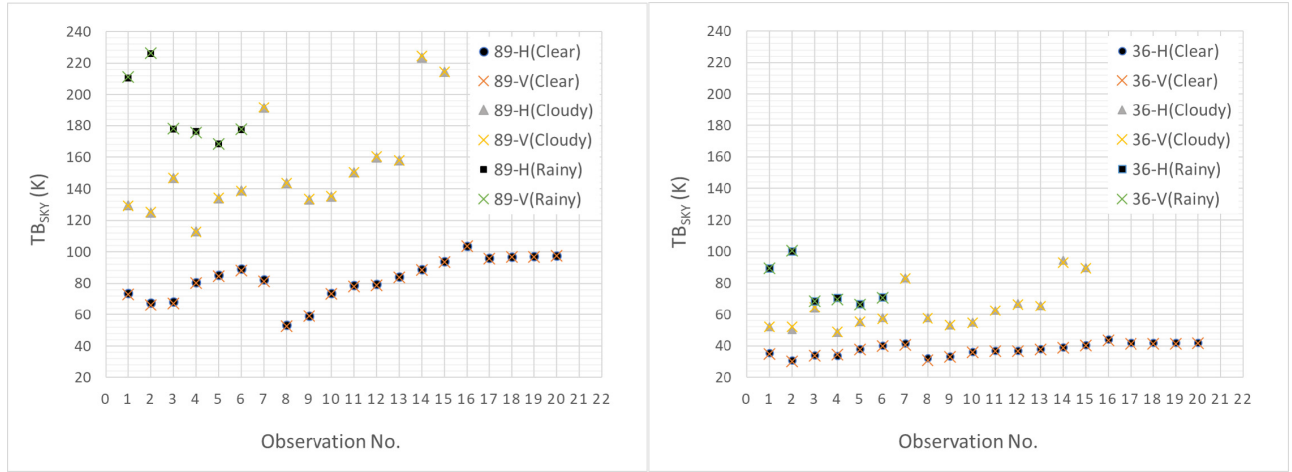


Fig. 9. Difference in the downward brightness temperature of the sky under different weather conditions. Observed frequencies are (Left) 89 and (Right) 36 GHz.

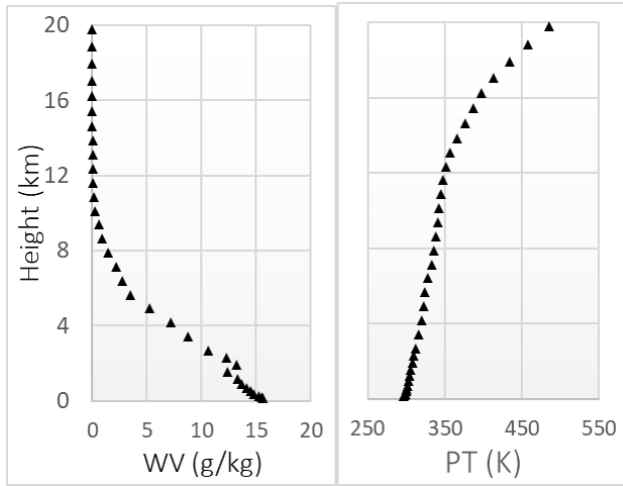


Fig. 10. Example of profiles of (Left) water vapor and (Right) potential temperature used in simulations.

of T'_{Bsky} on cloudy days were 153.1 and 153.2 for horizontal and vertical polarizations, respectively. T'_{Bsky} on cloudy days ranged from 112.6 to 224.6.

During light rain, T'_{Bsky} was above 170 K, and its maximum value was 226.2 K. The average value was about 189.5 K for both polarizations.

B. Errors in Observations

To estimate the error of target variables that are calculated from a combination of observed values, we used error propagation approach.

According to this approach, if the target variable Y is expressed as a function of variable x like

$$Y = f(x_1 + \sigma_1, x_2 + \sigma_2, x_3 + \sigma_3 \dots) \quad (\text{A1})$$

where σ is the observational error of variable x , and the error of Y (σ_Y) can be calculated in the following form:

$$\sigma_Y = \sqrt{\left(\frac{\partial f}{\partial x_1} \sigma_1\right)^2 + \left(\frac{\partial f}{\partial x_2} \sigma_2\right)^2 + \left(\frac{\partial f}{\partial x_3} \sigma_3\right)^2 \dots} \quad (\text{A2})$$

For each error (σ_1), we basically adopted standard deviation of observed values obtained from 100 samples for GBMR data

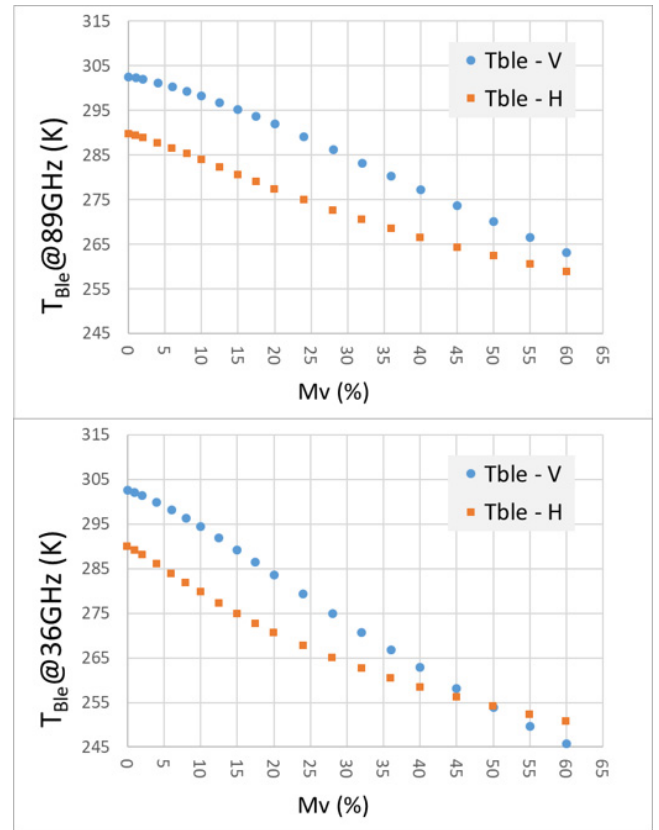


Fig. 11. Changes in the simulated brightness temperature of land emissions under various soil-moisture conditions simulated at (Top) 89 and (Bottom) 36 GHz.

and several-time measurements for soil moisture and land-surface temperature.

C. Atmospheric Profiles for the RTM

An example of the atmospheric profiles used for the atmospheric RTM in model simulations is shown in Fig. 10. The profiles were modified slightly based on the temperature rise due to latent heat and water vapor saturation within the cloud layer corresponding to the CWC distribution in comparison with that of the profile in the atmospheric model.

D. Simulated Brightness Temperatures of Land Emission

Fig. 11 shows the simulated results of the brightness temperatures of land emission. The results showed similar features to those of ground observations.

REFERENCES

- [1] C. W. O'Dell, F. J. Wentz, and R. Bennartz, "Cloud liquid water path from satellite-based passive microwave observations: A new climatology over the global oceans," *J. Climate*, vol. 21, no. 8, pp. 1721–1739, 2008, doi: [10.1175/2007JCLI1958.1](https://doi.org/10.1175/2007JCLI1958.1).
- [2] G. S. Elsaesser, C. W. O'Dell, M. D. Lebsock, R. Bennartz, T. J. Greenwald, and F. J. Wentz, "The multisensor advanced climatology of liquid water path (MAC-LWP)," *J. Climate*, vol. 30, no. 24, pp. 10193–10210, Dec. 2017, doi: [10.1175/JCLI-D-16-0902.1](https://doi.org/10.1175/JCLI-D-16-0902.1).
- [3] A. Lauer *et al.*, "Process-level improvements in CMIP5 models and their impact on tropical variability, the Southern Ocean, and monsoons," *Earth Syst. Dyn.*, vol. 9, no. 1, pp. 33–67, 2018, doi: [0.5194/esd-9-33-2018](https://doi.org/10.5194/esd-9-33-2018).
- [4] G. Liu and J. A. Curry, "Determination of characteristic features of cloud liquid water from satellite microwave measurements," *J. Geophys. Res.*, vol. 99, no. D10, pp. 20907–20928, 1994.
- [5] T. J. Greenwald, G. L. Stephens, T. H. V. Haar, and D. L. Jackson, "A physical retrieval of cloud liquid water over the global oceans using special sensor microwave/imager (SSM/I) observations," *J. Geophys. Res., Atmos.*, vol. 98, no. D10, pp. 18471–18488, Oct. 1993.
- [6] B. Lin and W. B. Rossow, "Observations of cloud liquid water path over oceans: Optical and microwave remote sensing methods," *J. Geophys. Res., Atmos.*, vol. 99, no. D10, pp. 20907–20928, 1994.
- [7] F. Weng and N. C. Grody, "Retrieval of cloud liquid water using the special sensor microwave imager (SSM/I)," *J. Geophys. Res., Atmos.*, vol. 99, no. D12, pp. 25535–25552, 1994.
- [8] C. Kummerow, W. S. Olson, and L. Giglio, "A simplified scheme for obtaining precipitation and vertical hydrometeor profiles from passive microwave sensors," *IEEE Trans. Geosci. Remote Sens.*, vol. 34, no. 5, pp. 1213–1232, Sep. 1996.
- [9] K. A. Hilburn and F. J. Wentz, "Intercalibrated passive microwave rain products from the unified microwave ocean retrieval algorithm (UMORA)," *J. Appl. Meteorol. Climatol.*, vol. 47, no. 3, pp. 778–794, Mar. 2008.
- [10] S. A. Ackerman *et al.*, "Satellites see the world's atmosphere," *Century Prog. Atmos. Rel. Sci., Celebrating Amer. Meteorol. Soc. Centennial, Meteorol. Monographs*, vol. 59. Washington, DC, USA: AMS, 2019, pp. 4.1–4.53.
- [11] T. J. Greenwald, R. Bennartz, M. Lebsock, and J. Teixeira, "An uncertainty data set for passive microwave satellite observations of warm cloud liquid water path," *J. Geophys. Res., Atmos.*, vol. 123, no. 7, pp. 3668–3687, Apr. 2018, doi: [10.1002/2017JD027638](https://doi.org/10.1002/2017JD027638).
- [12] R. Seto, T. Koike, and S. Kanae, "Representing cloud water content of extensive cloud systems over land using satellite-based passive microwave observations with a coupled land and atmosphere assimilation method," *J. Geophys. Res., Atmos.*, vol. 123, no. 22, pp. 12,829–12,856, 2018, doi: [10.1029/2018JD028864](https://doi.org/10.1029/2018JD028864).
- [13] F. Ulaby, R. K. Moore, and A. Fung, *Microwave Remote Sensing: Active and Passive: Microwave Remote Sensing Fundamentals and Radiometry*, vol. 1. Dedham, MA, USA: Artech House, 1986, p. 456.
- [14] M. Dobson, F. Ulaby, M. Hallikainen, and M. El-Rayes, "Microwave dielectric behavior of wet soil—Part II: Dielectric mixing models," *IEEE Trans. Geosci. Remote Sens.*, vol. GE-23, no. 1, pp. 35–46, Jan. 1985.
- [15] D. N. Kuria, T. Koike, H. Lu, H. Tsutsui, and T. Graf, "Field-supported verification and improvement of a passive microwave surface emission model for rough, bare, and wet soil surfaces by incorporating shadowing effects," *IEEE Trans. Geosci. Remote Sens.*, vol. 45, no. 5, pp. 1207–1216, May 2007.
- [16] NASA Earth Observations. *Land Surface Temperature*. Accessed: Mar. 7, 2020. [Online]. Available: https://earthobservatory.nasa.gov/global-maps/MOD_LSTD_M
- [17] F. T. Ulaby and D. G. Long, "Microwave interaction with atmospheric constituents," in *Microwave Radar and Radiometric Remote Sensing*. Ann Arbor, MI, USA: Univ. Michigan Press, 2014, pp. 324–365.
- [18] F. Ulaby, R. K. Moore, and A. Fung, *Microwave Remote Sensing: Active and Passive: From Theory to Application*, vol. 3. Dedham, MA, USA: Artech House, 1986, p. 1100.
- [19] E. G. Njoku and J.-A. Kong, "Theory for passive microwave remote sensing of near-surface soil moisture," *J. Geophys. Res.*, vol. 82, no. 20, pp. 3108–3118, 1977.
- [20] R. A. M. de Jeu, W. Wagner, T. R. H. Holmes, A. J. Dolman, N. C. van de Giesen, and J. Friesen, "Global soil moisture patterns observed by space borne microwave radiometers and scatterometers," *Surv. Geophys.*, vol. 29, nos. 4–5, pp. 399–420, Oct. 2008.
- [21] G. Liu, "A fast and accurate model for microwave radiance calculations," *J. Meteorol. Soc. Jpn. II*, vol. 76, no. 2, pp. 335–343, 1998.
- [22] K. Chen, T. D. Wu, L. Tsang, Q. Li, J. C. Shi, and A. K. Fung, "The emission of rough surfaces calculated by the integral equation method with a comparison to a three dimensional moment method simulation," *IEEE Trans. Geosci. Remote Sens.*, vol. 38, no. 1, pp. 249–256, Jan. 2001.



Rie Seto received the B.S., M.S., and Ph.D. degrees from the Department of Civil Engineering, University of Tokyo, Tokyo, Japan, in 2010, 2012, and 2015, respectively.

Since 2017, she has been an Assistant Professor with the Tokyo Institute of Technology, Tokyo. Her research interests include hydrometeorology, remote sensing, and monitoring and prediction of clouds over land.



Kentaro Aida received the B.E. and M.E. degrees from the Nagaoka University of Technology, Nagaoka, Japan, in 1998 and 2000, respectively, and the Ph.D. degree from the University of Tokyo, Tokyo, Japan, in 2017.

He has been a Research Specialist of the International Centre for Water Hazard and Risk Management (ICHARM), Tsukuba, Japan, under the auspices of United Nations Educational, Scientific and Cultural Organization (UNESCO) since July 2019. His research interests are soil moisture using the synthetic aperture radar and microwave radiometer.



Toshio Koike received the bachelor's, master's, and D.Eng. degrees from the University of Tokyo, Tokyo, Japan, in 1980, 1982, and 1985, respectively.

He was with the University of Tokyo, as a Research Associate in 1985 and a Lecturer from 1986 to 1987, and the Nagaoka University of Technology, Nagaoka, Japan, as an Associate Professor from 1988 to 1999 and a Professor in 1999. In 1999, he joined the Department of Civil Engineering, University of Tokyo, where he held the position of Professor until 2017. He is the Executive Director of the International Centre for Water Hazard and Risk Management (ICHARM), Tsukuba, Japan, under the auspices of United Nations Educational, Scientific and Cultural Organization (UNESCO) and Professor Emeritus of the University of Tokyo. His research interests are in hydrology, water resources, satellite remote sensing, climate change, and Asian monsoons.

Dr. Koike was a Council Member of the Science Council of Japan, Cabinet Office, and he has also helped to improve and develop various aspects of science nationwide since 2017 via the provision of policy recommendations to the government and the public. He has been the Chair of the River Council of Japan since 2015 and led discussions on important river-related matters to advise the Minister of Land, Infrastructure, Transport and Tourism of Japan.



Shinjiro Kanae received the B.S., M.S., and Ph.D. degrees from the Department of Civil Engineering, University of Tokyo, Tokyo, Japan, in 1994, 1996, and 1999, respectively.

He is a Professor with the Department of Civil and Environmental Engineering, Tokyo Institute of Technology, Tokyo. His research interests include terrestrial hydrology including river flood simulation, global water resources assessment, and climate change impact and adaptation research. He was a Lead Author for Chapter 3 of a special report on extremes and adaptation (SREX) by Intergovernmental Panel on Climate Change (IPCC), in 2012, and a Contributing Author (Chapter 3 "Freshwater") to the IPCC's Working Group II Contribution to AR5, in 2014.